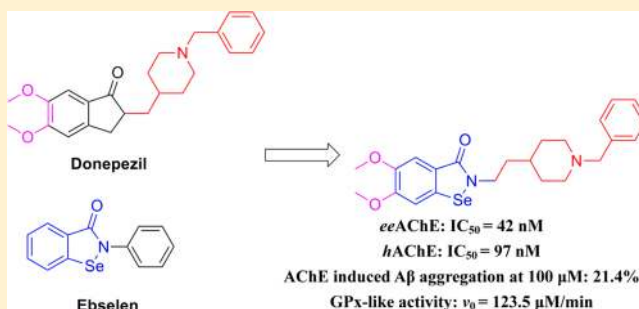# Synthesis and Evaluation of Multi-Target-Directed Ligands against Alzheimer's Disease Based on the Fusion of Donepezil and Ebselen

Zonghua Luo, Jianfei Sheng, Yang Sun, Chuanjun Lu, Jun Yan, Anqiu Liu, Hai-bin Luo, Ling Huang,* and Xingshu Li*

School of Pharmaceutical Sciences, Sun Yat-sen University, Guangzhou 510006, China

S Supporting Information

ABSTRACT: A novel series of compounds obtained by fusing the cholinesterase inhibitor donepezil and the antioxidant ebselen were designed as multi-target-directed ligands against Alzheimer's disease. An in vitro assay showed that some of these molecules did not exhibit highly potent cholinesterase inhibitory activity but did have various other ebselen-related pharmacological effects. Among the molecules, compound **7d**, one of the most potent acetylcholinesterase inhibitors (IC$_{50}$ values of 0.042 μM for *Electrophorus electricus* acetylcholinesterase and 0.097 μM for human acetylcholinesterase), was found to be a strong butyrylcholinesterase inhibitor (IC$_{50}$ = 1.586 μM), to possess rapid H$_2$O$_2$ and peroxynitrite scavenging activity and glutathione peroxidase-like activity (ν_0 = 123.5 μM min^{-1}), and to be a substrate of mammalian TrxR. A toxicity test in mice showed no acute toxicity at doses of up to 2000 mg/kg. According to an in vitro blood–brain barrier model, **7d** is able to penetrate the central nervous system.

*ee*AChE: IC$_{50}$ = 42 nM
*h*AChE: IC$_{50}$ = 97 nM
AChE induced Aβ aggregation at 100 μM: 21.4%
GPx-like activity: ν_0 = 123.5 μM/min

INTRODUCTION

Alzheimer's disease (AD), the most common form of dementia associated with progressive loss of memory, speech, and recognition, occurs most frequently in elderly people. It has been estimated that 36 million people were living with dementia in the world in 2010 and that the number will double every 20 years, leading to more than 115 million people with AD in 2050.[1] The etiology of AD is not fully known, but some hallmarks, such as low levels of acetylcholine, β-amyloid (Aβ) deposits, τ-protein aggregation, oxidative stress, inflammation, and dyshomeostasis of biometals, are considered to play important roles in the pathogenesis of this disease.[2] Many different approaches to the treatment of AD have been developed over the past several decades. At present, there is no drug that can definitively cure Alzheimer's disease, and the primary therapeutic options currently approved by the U.S. Food and Drug Administration for the treatment of AD are acetylcholinesterase inhibitors (AChEIs), namely, tacrine, donepezil, rivastigmine, and galantamine. Among them, donepezil is the most effective pharmacological agent for AD treatment.[3,4] However, it is effective in reversing the symptoms for only a short period of time.

In recent years, accumulated evidence has indicated that the most successful treatment strategy will likely incorporate a sequential, multifactorial approach to this multifaceted disease, termed the multi-target-directed ligand (MTDL) strategy.[5] The "one-molecule, multiple-targets" paradigm is effective in treating complex diseases because of the ability of the drug to interact with multiple targets responsible for disease pathogenesis. Thus, interest in the development of MTDLs has

become heightened.[6–11] Given the complex nature of AD and the fact that a single drug acting on a specific target (AChE) may have undesirable clinical effects, a variety of MTDLs acting on very diverse targets have been developed by many research groups.[12–15]

Selenium (Se) is an essential trace mineral nutrient with multiple roles in the growth and function of living animal cells. Twenty-five selenoproteins in the human body exert specific biological functions.[16] Moreover, the mineral is known to provide protection from free radical-induced cell damage.[17] In humans, selenium levels decrease with age, and there are considerable data showing that selenium might play different roles in the progression of AD.[18,19] There has been a heightened interest in the role of this trace element in health and neurological disorders in recent years.[20–23] Some animal experiments indicate that organoselenium has a higher biodisposability and biological activity than Se in inorganic compounds.[24] Recently, diphenyl diselenide [(PhSe)$_2$] and *p,p'*-methoxyldiphenyl diselenide [(MeOPhSe)$_2$] were studied for the treatment of a sporadic Alzheimer's-type dementia in a rat model, and the results demonstrated that (MeOPhSe)$_2$ dietary supplementation reversed streptozotocin-induced memory impairment.[25,26]

Ebselen [2-phenyl-1,2-benzisoselenazol-3(2H)-one] is a lipid-soluble cyclic selenenamide and a classic example of a glutathione peroxidase (GPx) mimic,[27] and it protects cells by catalyzing the reduction of peroxides with glutathione. Ebselen

has also been demonstrated to be a substrate for human thioredoxin reductase.[28−30] It inhibits nonenzymatic and enzymatic lipid peroxidation in cells and has anti-inflammatory activity in various animal models. Because of its anti-inflammatory activity, ebselen has been used in the treatment of patients with acute ischemic stroke or delayed neurological deficits after aneurismal subarachnoid hemorrhage. A recent study indicates that ebselen could be used as a potential anti-AD agent on the basis of its ability to inhibit iron-induced tau phosphorylation.[31]

Because the pharmacological effects of ebselen, including its antioxidant and anti-inflammatory activities, are closely related to the etiology of AD, our design principle involved the fusion of the important pharmacophores of donepezil and ebselen in a new molecule, "selenpezil", without the major structural modifications (Figure 1) like those of other MTDLs.[32] The hybrid compounds possess strong AChE inhibitory activity and many of the pharmacological effects of ebselen.
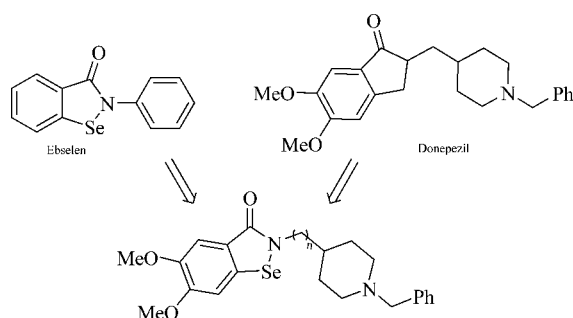

Figure 1. Drug design strategy for multi-target-directed ligands.

■ RESULTS AND DISCUSSION

Chemistry. Amine intermediates **4a−e** were obtained as reported in the literature (see the Supporting Information), and target compounds **5a−d**, **6a−d**, **7a−d**, **8**, and **9** were synthesized according to the synthetic approaches in Scheme 1.

With various amine intermediates available, the target molecules were easily synthesized by the route shown in Scheme 1. The diazotization of *o*-aminobenzoic acid or its analogues and their subsequent reaction with Na_2Se_2 provided diselenium intermediate **2**. Compound **2** reacted with thionyl
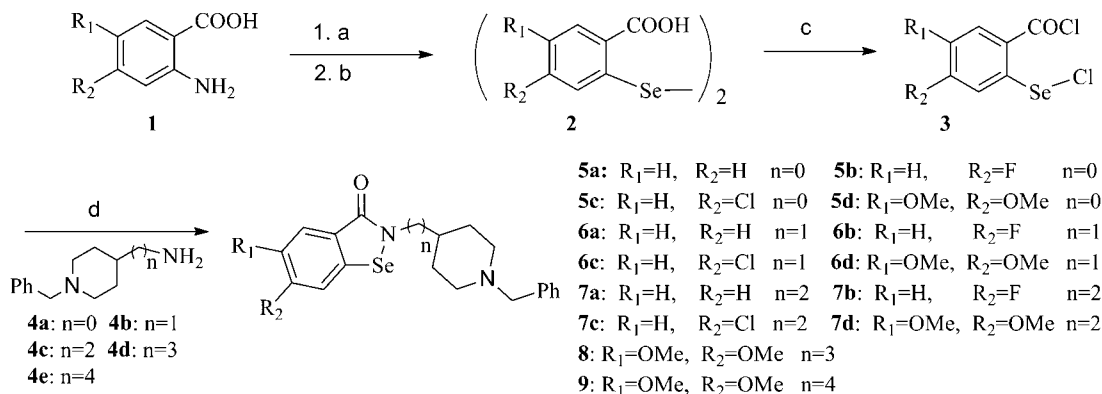
chloride and the amine intermediates efficiently to provide the target compounds in good yields.

One of the possible metabolic products of selenide in vivo is selenoxide. To evaluate the biological activity of the metabolic products, we prepared selenoxide **10** by the oxidation of **7d** with 1.5 equiv of H_2O_2 at room temperature (Scheme 2).

In Vitro Inhibition Studies of AChE and BuChE. To evaluate the potential application of target compounds **5a−d**, **6a−d**, **7a−d**, **8**, **9**, and **10** for the treatment of AD, we determined their levels of AChE inhibitory activity by the method of Ellman et al.,[33] using donepezil and ebselen as reference standards (Table 1). Among these compounds, **7d**, **8**, and **9**, in which the piperidine groups were linked to the 5,6-dimethoxybenzoselenazol-3(2H)-one moiety by two-, three-, and four-carbon spacers, respectively, exhibited more potent inhibition of AChE than other analogues (IC$_{50}$ values of 0.042, 0.072, and 0.038 μM for **7d**, **8**, and **9**, respectively). Structure−activity relationship analysis showed that the methoxy group in the benzoselenazol-3(2H)-one moiety is necessary for inhibitory activity. Compounds **7a**, **7b**, and **7c**, whose methoxy groups (R$_1$ and R$_2$) were replaced by H, F, and Cl, respectively, exhibited weaker inhibitory activities than **7d** (**7a**, R$_1$ = R$_2$ = H, IC$_{50}$ = 0.382 μM; **7b**, R$_1$ = H, R$_2$ = F, IC$_{50}$ = 0.224 μM; **7c**, R$_1$ = H, R$_2$ = Cl, IC$_{50}$ = 0.206 μM; **7d**, R$_1$ = R$_2$ = OCH$_3$, IC$_{50}$ = 0.042 μM). The length of the alkylene chain, especially with zero to two carbons, is also important for inhibitory activity. Compounds **5d**, **6d**, and **7d**, with or without the one- and two-carbon spacers between the 5,6-dimethoxybenzoselenazol-3(2H)-one moiety and the piperidine group, exhibited IC$_{50}$ values of 11.84, 4.231,M and 0.042 μM, respectively. The inhibitory activities of compounds **7d**, **8**, **9**, and **10** against human AChE were determined using same method, with donepezil as the reference. Via comparison of the results with AChE from the electric eel, slightly weaker activities were observed (Table) (IC$_{50}$ values of 0.097, 0.231, 0.103, and 0.163 μM for **7d**, **8**, **9**, and **10**, respectively).

In recent years, numerous studies[34−37] have indicated that butyrylcholinesterase (BuChE) levels are unchanged or even increase in advanced AD while AChE activity in certain brain regions decreases. These studies implied that a balance of inhibition of both AChE and BuChE may be beneficial in treating the cognitive deficits observed in AD. Therefore, the inhibitory activity of these compounds against BuChE was also evaluated, and the results are listed in Table 1. The majority of the compounds exhibited good BuChE inhibitory activities.

Scheme 1. Synthesis of Target Compounds 4a−d, 5a−d, 6a−d, 7, and 8[a]

5a: R$_1$=H, R$_2$=H n=0　**5b**: R$_1$=H, R$_2$=F n=0
5c: R$_1$=H, R$_2$=Cl n=0　**5d**: R$_1$=OMe, R$_2$=OMe n=0
6a: R$_1$=H, R$_2$=H n=1　**6b**: R$_1$=H, R$_2$=F n=1
6c: R$_1$=H, R$_2$=Cl n=1　**6d**: R$_1$=OMe, R$_2$=OMe n=1
7a: R$_1$=H, R$_2$=H n=2　**7b**: R$_1$=H, R$_2$=F n=2
7c: R$_1$=H, R$_2$=Cl n=2　**7d**: R$_1$=OMe, R$_2$=OMe n=2
8: R$_1$=OMe, R$_2$=OMe n=3
9: R$_1$=OMe, R$_2$=OMe n=4

4a: n=0 **4b**: n=1
4c: n=2 **4d**: n=3
4e: n=4

[a]Reagents and conditions: (a) NaNO$_2$, HCl; (b) Na$_2$Se$_2$; (c) SOCl$_2$, reflux; (d) (Et)$_3$N, CH$_2$Cl$_2$.

Scheme 2. Synthesis of Selenoxide 10[a]
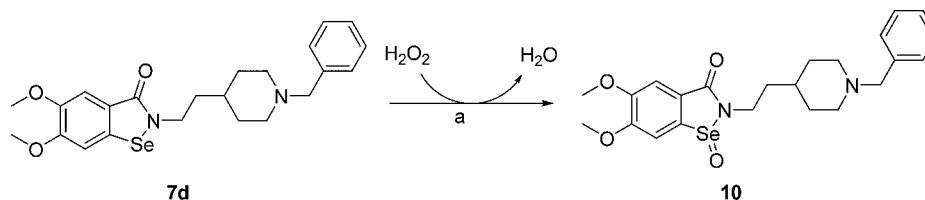
[a]Reagents and conditions: (a) 1.5 equiv of H_2O_2, CH_2Cl_2, room temperature.

Table 1. Inhibition of AChE from *Electrophorus electricus* (*ee*AChE) and Human Erythrocytes (*h*AChE), BuChE from Equine Serum, and Human Recombinant AChE-Induced Aβ Aggregation by the Target Compounds

compd	R_1	R_2	n	IC$_{50}$ (μM) ± SD		selectivity for AChE[c]	IC$_{50}$ (μM) ± SD	% inhibition of AChE-induced Aβ$_{1-40}$ aggregation[f]
				*ee*AChE[a]	*eq*BuChE[b]		*h*AChE[d]	
5a	H	H	0	17.58 ± 1.3	8.316 ± 0.446	0.47	nd[e]	nd[e]
5b	H	F	0	19.72 ± 1.4	10.58 ± 0.762	0.54	nd[e]	nd[e]
5c	H	Cl	0	10.10 ± 0.3	21.52 ± 1.445	2.13	nd[e]	nd[e]
5d	OCH$_3$	OCH$_3$	0	11.84 ± 0.8	9.463 ± 0.768	0.80	nd[e]	nd[e]
6a	H	H	1	19.80 ± 0.7	3.628 ± 0.015	0.18	nd[e]	nd[e]
6b	H	F	1	12.27 ± 0.4	3.461 ± 0.150	0.28	nd[e]	nd[e]
6c	H	Cl	1	6.160 ± 0.5	2.295 ± 0.085	0.37	nd[e]	nd[e]
6d	OCH$_3$	OCH$_3$	1	4.231 ± 0.10	3.921 ± 0.096	0.93	nd[e]	nd[e]
7a	H	H	2	0.382 ± 0.012	2.132 ± 0.166	5.58	nd[e]	nd[e]
7b	H	F	2	0.224 ± 0.016	3.668 ± 0.100	16.4	nd[e]	nd[e]
7c	H	Cl	2	0.206 ± 0.026	2.346 ± 0.023	11.4	nd[e]	nd[e]
7d	OCH$_3$	OCH$_3$	2	0.042 ± 0.003	1.586 ± 0.075	36.7	0.097 ± 0.007	21.4 ± 2.0
8	OCH$_3$	OCH$_3$	3	0.072 ± 0.002	1.503 ± 0.150	20.9	0.231 ± 0.03	26.3 ± 4.0
9	OCH$_3$	OCH$_3$	4	0.038 ± 0.002	0.517 ± 0.004	13.6	0.103 ± 0.01	46.3 ± 9.3
10				0.043 ± 0.001	1.362 ± 0.073	31.7	0.163 ± 0.01	nd[e]
donepezil				0.038 ± 0.003	3.365 ± 0.058	88.6	0.011 ± 0.001	21.1 ± 3.3
tacrine				0.113 ± 0.012	0.015 ± 0.002	0.13	0.534 ± 0.022	10.3 ± 2.8
ebselen				41.01 ± 0.672	10.368 ± 0.035	0.25	nd[e]	nd[e]

[a]The 50% inhibitory concentration (means ± SD of three experiments) of AChE from electric eel. [b]The 50% inhibitory concentration (means ± SD of three experiments) of BuChE from equine serum. [c]Selectivity for AChE = IC$_{50}$(*eq*BuChE)/IC$_{50}$(*ee*AChE). [d]The 50% inhibitory concentration (means ± SD of three experiments) of AChE from human erythrocytes. [e]Not determined. [f]Inhibition of human recombinant AChE-induced Aβ$_{1-40}$ aggregation produced by the tested compound at 100 μM.

Compound **9**, which had the best AChE inhibitory activity, also showed the best BuChE inhibitory activity (IC$_{50}$ value of 0.517 μM). The structure−activity relationship between the length of the alkylene chain and AChE inhibitory activity was also observed for BuChE inhibitory activity. The effect of the methoxy group observed with AChE inhibitory activity, however, was not apparent with BuChE inhibitory activity. It is notable that compound **10**, one of the possible metabolic products of **7d**, exhibited inhibitions similar to those of AChE and BuChE (IC$_{50}$ values of 0.042 μM for AChE and 1.586 μM for BuChE).

Kinetic Characterization of AChE Inhibition. Considering the requirement of the calculated logarithm of the octanol−water partition coefficient (clogP) in Lipinski's rules, compound **7d** (clogP = 4.611), one of the most potent AChE inhibitors, was selected to further study the inhibitory mechanism of AChE. The graphical presentation of the steady-state inhibition data of compound **7d** for AChE is shown in

Figure 2. The intersection point of the Lineweaver−Burk reciprocal plot fell in the second quadrant, which is indicative of mixed-type inhibition. The competitive inhibition constant (K_i) of **7d** is 0.017 ± 0.003 μM.

Docking Study of Compounds 7d and 10 with AChE. To evaluate the binding modes of the compounds with respect to AChE, compound **7d** was selected for docking simulations using the CDOCKER program in Discovery Studio version 2.1 based on the X-ray crystal structure of the complex of the *Torpedo californica* enzyme (*Tc*AChE) and donepezil (Protein Data Bank entry 1EVE).[38] The position of compound **7d** with respect to the key residues in the binding site is shown in Figure 3A. The results suggest that **7d** binds in the central catalytic pocket and the peripheral anionic site (PAS) along the active site gorge of the enzyme with its three major functional groups, the phenyl ring and the carbonyl group on the dimethoxybenzo[*d*][1,2]selenazol-3(2*H*)-one moiety and the phenyl ring of the *N*-benzyl group moiety. The phenyl ring with
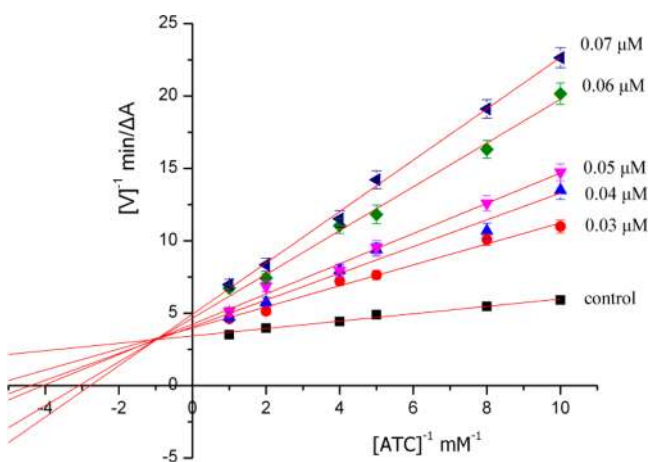
Figure 2. Kinetic study of the mechanism of *ee*AChE inhibition by compound **7d**. Overlaid Lineweaver−Burk reciprocal plots of the AChE initial velocity at increasing substrate concentrations (0.1−1 mM) in the absence of inhibitor and in the presence of **7d** are shown. Lines were derived from a weighted least-squares analysis of the data points. The experimental data are the means ± SD of three independent experiments.
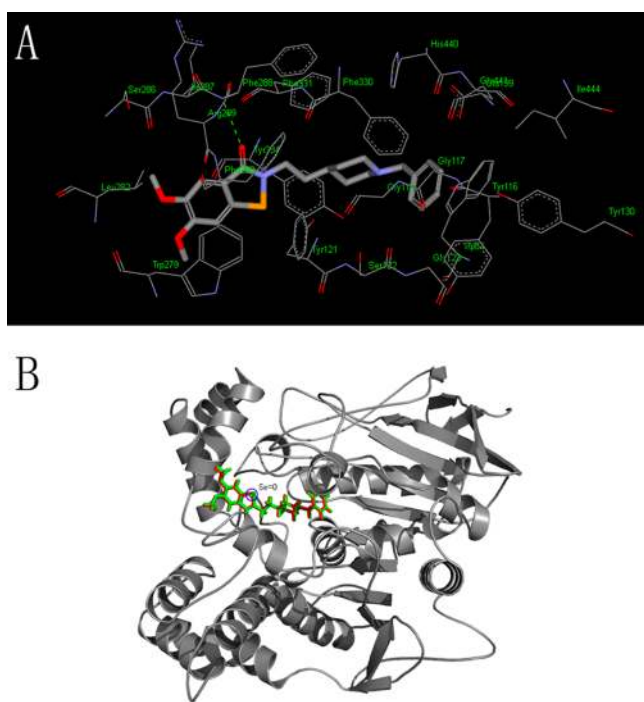

Figure 3. Docking models of the compound−enzyme complex. (A) Representation of compound **7d** docked into the binding site of AChE highlighting the protein residues that form the main interactions with the inhibitor. The hydrogen bonding interaction between the ligand and Arg289 is shown as a green line. (B) Overlap of **7d** and **10** docked with AChE.

the dimethoxy group is stacked above the peripheral anionic site (PAS) residue Trp279 (4.327 Å). The piperidine ring is located on the aromatic gorge connecting the PAS and CAS (catalytic binding site). The carbonyl oxygen of **7d** interacts with Phe288 via a hydrogen bond (NH of Phe288 to O14 of **7d**). The phenyl ring of the *N*-benzyl forms a π-stacking interaction with the indole ring of Trp84 (4.297 Å). A docking simulation of selenoxide **10** was also performed. The overlap of

7d and **10** in AChE indicates that the selenoxide group does not affect the binding mode, which agrees with the in vitro activity assay (Figure 3B).

Inhibition of Human Recombinant AChE-Induced Aβ$_{1−40}$ Aggregation. Mounting evidence[39,40] has indicated that AChE colocalizes with Aβ in senile plaques, promoting the assembly of Aβ into fibrils and accelerating Aβ peptide deposition. It has been suggested that AChE achieves its aggregation-promoting action through direct binding with Aβ via its peripheral binding site. Inhibition of the peripheral site might prevent the Aβ peptide aggregation induced by AChE.[41] On the basis of the results of the kinetic and docking studies, compound **7d** could act as a dual-binding site AChE inhibitor. Therefore, we selected **7d**, **8**, and **9** for evaluation of their ability to inhibit Aβ$_{1−40}$ aggregation induced by human recombinant AChE using a thioflavin T-based fluorometric assay[42] (Table 1). The results showed that the selected compounds were more effective inhibitors of AChE-induced Aβ$_{1−40}$ aggregation than tacrine (10.3%) and donepezil (21.1%), with 21.4−46.3% inhibition at 100 μM. The results also showed that a longer linker between the 5,6-dimethoxybenzoselenazol-3(2*H*)-one moiety and the piperidine group was favorable for inhibition.

Glutathione Peroxidase-like Activity. Glutathione peroxidase (GPx) plays a crucial role in the detoxification of hydroperoxides in aerobic living organisms. It catalytically reduces harmful peroxides by reducing glutathione (GSH) or other thiols and protects the lipid membranes and other cellular components from oxidative damage.

The GPx-like catalytic activity of compounds **7d** and **8−10** was studied using GSH as a thiol cofactor and hydrogen peroxide (H_2O_2) as the substrate. The initial rates ($ν_0$) were determined for the reduction of peroxide at a concentration of 80 μM for all the tested compounds. The results listed in Table 2 showed that **7d** (123.5 μM min^{-1}) exhibited GPx-like activity

Table 2. Initial Rates for the Reduction of H$_2$O$_2$ by GSH in the Presence of Ebselen, 7d, 8, 9, 10, and Donepezil

compd	$ν_0$ (μM min^{-1})^{a,b}
control^b	49.5 ± 2.6
7d	123.5 ± 10.9
8	86.1 ± 3.0
9	80.1 ± 2.8
10	97.1 ± 4.3
ebselen	121.3 ± 1.1
donepezil	46.1 ± 3.2

^{a}Reactions were conducted in phosphate buffer (100 mM) (pH 7.5) with 1 mM ethylenediaminetetraacetate (EDTA), 2 mM GSH, 0.4 mM NADPH, 1.3 unit/mL glutathione reductase (GR), 80 μM selenium compounds, and 1.6 mM H$_2$O$_2$. The control values were obtained from the reduction of H$_2$O$_2$ by GSH in the absence of the compound. ^{b}All values were determined in triplicate for the initial 10 s, and the average values with the standard deviation are reported.

similar to that of ebselen (121.3 μM min^{-1}) but compounds **8**, **9**, and **10** had lower activities than ebselen. GPx-like activity was associated with the length of the linker between the ebselen moiety and benzylpiperidine (**7d**, $n = 2$, $ν_0 = 123.5$ μM min^{-1}; **8**, $n = 3$, $ν_0 = 86.1$ μM min^{-1}; **9**, $n = 3$, $ν_0 = 80.1$ μM min^{-1}). Not surprisingly, selenoxide **10** still exhibited potent GPx-like activity (97.1 μM min^{-1}), but donepezil (46.1 μM min^{-1}) exhibited no activity compared to the control (49.5 μM min^{-1}).

Hydrogen Peroxide Scavenging Activity. Oxidative stress is an early feature of AD pathology, and during the aging process, oxidation-induced apoptosis and increased activity of β- and γ-secretases may contribute to the generation of Aβ. The antioxidant protection provided by removing reactive oxygen species (ROS), such as hydrogen peroxide, is important in older individuals, especially AD patients, because the endogenous antioxidant protection system declines rapidly with age. To evaluate the antioxidant activity of the donepezil and ebselen derivatives, compounds **7d**, **8**, **9**, and **10** were selected for the ferrous ion oxidation−xylenol orange (FOX) assay,[43] and donepezil and ebselen were used as reference compounds. The results in Figure 4 indicate that ebselen and
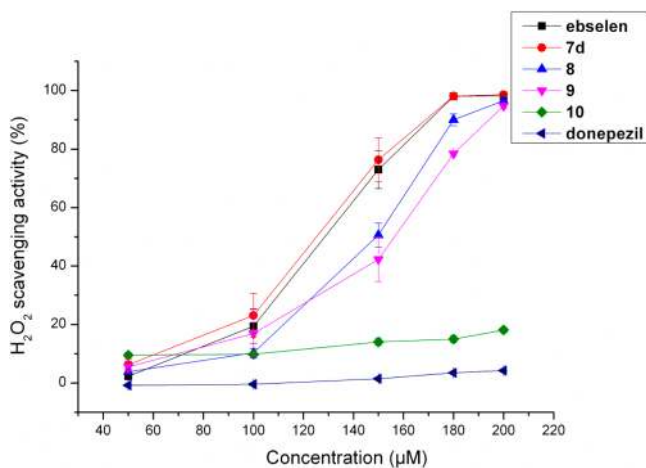

Figure 4. Scavenging effects on hydrogen peroxide in the FOX assay (100 μM H$_2$O$_2$). Values reported are means ± SD of three independent experiments. $P < 0.01$ in comparison to donepezil.

7d show similar scavenging activities for hydrogen peroxide at high concentrations, but **7d** showed improved scavenging activity at lower concentrations. Compounds **8** and **9** showed scavenging activities lower than that of ebselen. Moreover, selenoxide **10** demonstrated minimal antioxidant activity. Donepezil showed very weak activity, even at high concentrations.

Peroxynitrite Scavenging Activity. Peroxynitrite, which is generated by the diffusion-limited reaction of nitric oxide and the superoxide anion, has been detected in macrophages[44] and endothelial cells.[45] Peroxynitrite is a strong oxidizing and nitrating agent. Oxidation reactions include DNA damage leading to base modification and mutations; single- and double-stranded breaks;[46,47] one- or two-electron oxidations of sulfhydryl leading to thiyl radical formation and transmission, which results in the depletion of thiol pools;[48] lipid peroxidation; and the hydroxylation of phenols.[49,50] Antioxidants that may provide additional endogenous cellular defenses against this species are of obvious interest.

The antioxidant activities of test compounds against peroxynitrite were determined using the method reported by Balavoineet et al.[51] Peroxynitrite formation, resulting in the bleaching of Evans blue (EB) dye, was measured at 608 nm (ε = 70000 M^{-1} cm^{-1}). Consumption of Evans blue dye, with or without different concentrations of the test compound, was the basis for the calculated amount of peroxynitrite. D_0 and D_{TC} are the stoichiometries for the reaction of peroxynitrite with Evans blue dye without and with the test compound, respectively. The

k_{TC}/k_{EB} ratio could be calculated from the slope of the line generated by plotting $\Delta[TC]_0/\Delta[EB]$ against $[TC]/[EB]$. For the sake of simplicity, initial concentrations $[TC]_0$ and $[EB]_0$ were used in the calculations. In this work, instead of $\Delta[EB]$, we measured the stoichiometry $D = \Delta[EB]/\Delta[NaOONO^{3-}]$ to avoid the effect of slight deviations in peroxynitrite concentration. The D_0/D_{TC} ratio is equivalent to $\Delta[TC]_0/\Delta[EB]_a$, where D_0 and D_{TC} are the reaction stoichiometries in the absence and presence of the test compound, respectively. The D_0/D_{TC} values for different concentrations of antioxidant were plotted against $[TC]_0/[EB]_0$ (Figure 5). Antioxidant
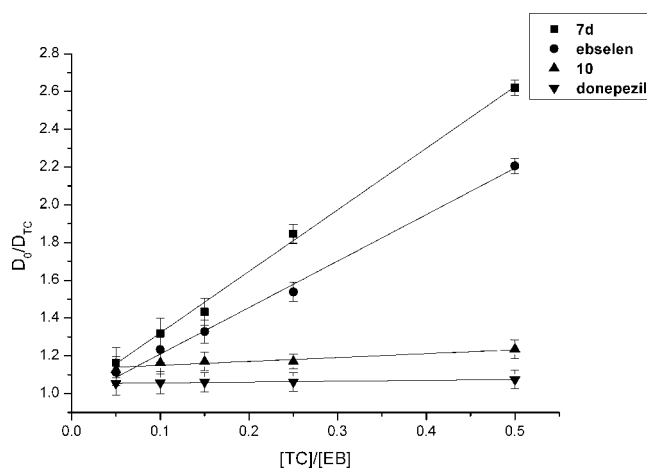

Figure 5. D_0/D_{TC} for different concentrations of test compounds plotted vs $[TC]/[EB]$. The reaction conditions were as follows: room temperature, phosphate buffer (50 mM), pH 7.4, and $[EB]_0 = 20$ μM. $P < 0.01$ comparing **7d** and ebselen with donepezil; $P < 0.05$ comparing **10** with donepezil.

activity was measured as the slope of the straight line (k_{TC}/k_{EB}). As indicated, compound **7d** exhibited the most potent antioxidant activity of all of the test compounds (k_{TC}/k_{EB} values of 3.28 ± 0.11, 2.42 ± 0.08, and 0.21 ± 0.01 for **7d**, ebselen, and **10**, respectively). In contrast, donepezil showed negligible activity under the same conditions ($k_{TC}/k_{EB} = 0.04 \pm 0.004$).

Compound 7d Is a Substrate of TrxR. Thioredoxin reductase (TrxR) is a selenoenzyme that catalyzes the reduction of thioredoxin (Trx) using NADPH as an electron source. Maintaining full TrxR activity by adequate dietary selenium intake has been proposed for the prevention of several cardiovascular and neurological disorders.[52] Organoselenium compounds can be metabolized by TrxR to form selenol intermediates[28,29,53,54] that can imitate the function of antioxidant selenoenzymes.[55,56]

For this study, compound **7d** was used according to the method of Zhao and Holmgren[28] to investigate the ability of donepezil−ebselen hybrids to serve as substrates of TrxR. Ebselen and donepezil were used as reference compounds. The measurements were performed in buffer containing 50 mM Tris-HCl, 1 mM EDTA, 100 μM NADPH, and 15 μM test compound. The reactions were started via the addition of TrxR to a final volume of 0.2 mL. The results shown in Figure 6 indicate that compound **7d** and ebselen are substrates of mammalian TrxR but that donepezil is not. Compound **7d** and ebselen show similar activities, as shown in Table 3.

In Vitro Blood−Brain Barrier Permeation Assay. Brain penetration is a major requirement for successful CNS drugs.
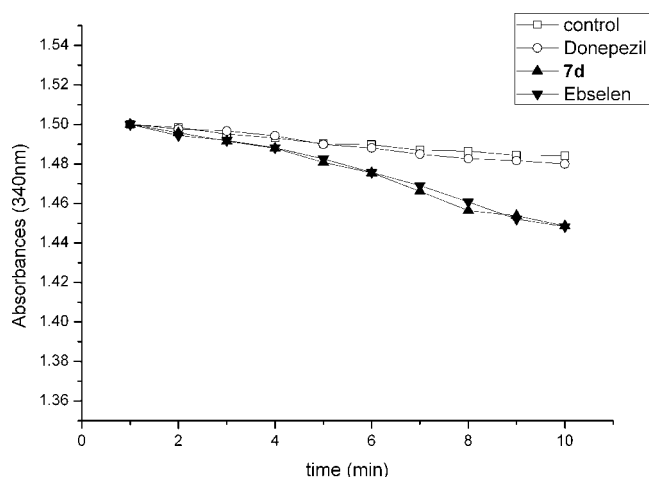
Figure 6. Reduction of compounds by NADPH catalyzed by mammalian thioredoxin reductase (TrxR). Test compounds at concentrations of 15 μM in 0.2 mL of 50 mM Tris-HCl and 1 mM EDTA (pH 7.5), containing 100 μM NADPH, were mixed with thioredoxin reductase from rat liver, and the absorbance at 340 nm (A_{340}) was measured against an identical blank with enzyme but without test compounds.

Table 3. Comparative Reduction of 7d, Donepezil, and Ebselen by Thioredoxin Reductase (TrxR) from Rat Liver

compd	ΔAbs$_{340}$ (NADPH oxidation/min)[a]	activity[b]
control	0.0158 ± 0.0014	1.0 ± 0.09
donepezil	0.019 ± 0.0017	1.20 ± 0.11
7d	0.0514 ± 0.0021	3.25 ± 0.13
ebselen	0.0517 ± 0.0033	3.27 ± 0.21

[a]Data are expressed as the means ± SD for three or more independent experiments. Calculations were performed using a concentration of 15 μM for all tested compounds. [b]Relative activities were calculated in relation to the control (arbitrary value of 1.00) activity determined in the absence of test compounds.

To evaluate the brain penetration of our new compounds, we used a parallel artificial membrane permeation assay for the blood−brain barrier (PAMPA-BBB), as recently described by Di et al.[57] We compared the permeability of 13 commercial drugs with reported values to validate the assay (Table S8 of the Supporting Information). A plot of experimental data versus reported values produced a good linear correlation, P_e(exp) = 1.4574P_e(bibil) − 1.0773 (R^2 = 0.9427) (see Figure S1 of the Supporting Information). From this equation and considering the limit established by Di et al. for blood−brain barrier permeation, we determined that compounds with permeabilities above 4.7 × 10^{-6} cm s^{-1} could cross the blood−brain barrier (see Table S9 of the Supporting Information). The selected compounds were then tested in the PAMPA-BBB assay, and the results are presented in Table 4. Thus, it is expected that they could penetrate into the CNS and reach their biological targets located in the CNS.

Acute Toxicity of Compound 7d. The acute toxicity profile is considered to be a very important criterion in the development of new drugs. Compound **7d**, which was perhaps the most promising multifunctional anti-AD agent, was tested in this assay. Twenty KM mice were randomly divided into four groups, and the test compound was given in single oral doses of 0, 677, 1333, and 2000 mg/kg. After administration of the compound, mice were observed continuously for the first 4 h

Table 4. Permeabilities in the PAMPA-BBB Assay for the Selected Compounds and Their Predicted Penetration into the CNS

compd[a]	P_e (×10^{-6} cm s^{-1})[b]	prediction
7d	8.6 ± 0.8	CNS+
8	10.3 ± 0.8	CNS+
9	15.8 ± 1.0	CNS+
chlorpromazine	6.0 ± 0.3	CNS+

[a]Compounds were dissolved in DMSO at a concentration of 5 mg/mL and diluted with a PBS/EtOH mixture (70:30). [b]Values are expressed as the means ± SD of three independent experiments.

for any abnormal behavior and mortality changes, intermittently for the next 24 h, and occasionally thereafter for 14 days for the onset of any delayed effects. All mice were sacrificed on the 14th day after drug administration and examined macroscopically for possible damage to the heart, liver, and kidneys. The results showed that the animals treated with compound **7d** did not show any acute toxicity and mortality either immediately or during the post-treatment period. Furthermore, no significant abnormal changes were observed during the experimental period in terms of water or food consumption or body weight. Therefore, compound **7d** proved to be nontoxic and well tolerated at doses of up to 2000 mg/kg.

■ CONCLUSION

In conclusion, our study involved the synthesis of a new series of multi-target-directed ligands for the treatment of AD that were produced by the fusion of donepezil and ebselen. These compounds were evaluated as potential multivalent inhibitors of ChE, as superfast antioxidant agents against H$_2$O$_2$ and peroxynitrite, and as GPx mimics. Among the synthesized compounds, compound **7d** exhibited very good inhibitory potency toward hAChE (IC$_{50}$ = 97 nM) and good GPx-like activity (123.5 μM min^{-1}). This compound is able to penetrate the CNS, according to an in vitro blood−brain barrier model, and toxicity tests in mice showed that **7d** has no acute toxicity at doses of up to 2000 mg/kg. These results showed that compound **7d** is a potential lead compound for the treatment of AD. Further investigations of AD therapeutic candidates based on these results are in progress.

■ EXPERIMENTAL SECTION

Chemistry. All reagents used in the synthesis were obtained commercially and used without further purification, unless otherwise specified. The ^{1}H NMR and ^{13}C NMR spectra were recorded using TMS as the internal standard on a Bruker BioSpin GmbH spectrometer at 400 and 101 MHz, respectively, and the coupling constants are reported in hertz. The reactions were followed by thin-layer chromatography (TLC) on glass-packed precoated silica gel plates and visualized in an iodine chamber or with a UV lamp. Flash column chromatography was performed using silica gel (200−300 mesh) purchased from Qingdao Haiyang Chemical Co. Ltd. The high-resolution mass spectra were obtained using a Shimadzu LCMS-IT-TOF mass spectrometer. The term "dried" refers to the use of anhydrous sodium sulfate. The purity (≥95%) of the samples was determined by high-performance liquid chromatography (HPLC), conducted on a Shimadzu LC-20AT series system, a TC-C18 column (4.6 mm × 250 mm, 5 μm), eluted with a 30:70 acetonitrile/PBS mixture [25 mM NaH$_2$PO$_4$ (pH 3.0)], at a flow rate of 0.5 mL/min.

General Procedure for the Synthesis of 2,2′-Diselenobisbenzoic Acid (2). 2-Aminobenzoic acid (0.1 mol) was added to a mixture of 37% HCl (20 mL) and H$_2$O (20 mL). After the mixture had cooled to 0 °C, a solution of sodium nitrite (0.11 mol, 30%) was added slowly,

and the reaction mixture was stirred for 30 min. The mixture was then slowly poured into an aqueous solution of disodium diselenide (0.05 mol), and the resulting solution was stirred at 50 °C for 2.5 h. After the mixture had cooled, hydrogen chloride was added until the pH reached <1. The solution was filtered and washed with H_2O, and the residue was dissolved in saturated $NaHCO_3$. The solution was stirred at 100 °C for 1 h. After the mixture had cooled, the pH was adjusted with HCl to a value of <1 to produce the product, which was separated by filtration.

General Procedure for the Synthesis of 3. 2,2′-Diselenobisbenzoic acid (**2**, 0.01 mol) was added to thionyl chloride (20 mL), and DMF (0.5 mL) was added as a catalyst. After the reaction mixture had been stirred at 85 °C for 3 h, the solvents were evaporated under a vacuum, and the crude products were purified by recrystallization from hexane.

General Procedure for the Synthesis of 5a−d, 6a−d, 7a−d, 8, and 9. A solution of **3** (2.5 mmol) in dry CH_2Cl_2 (5 mL) was added dropwise over 15 min at 0 °C to a stirred solution of the corresponding amine (2 mmol) in dry CH_2Cl_2 containing dry triethylamine (5 mmol). Stirring was continued for 5 h at room temperature. Water was added, and the mixture was extracted with CH_2Cl_2, dried, and filtered to produce the crude products, which were purified by column chromatography using silica gel and a CH_2Cl_2/MeOH mixture (58−82% yield).

2-(1-Benzylpiperidin-4-yl)benzo[d][1,2]selenazol-3(2H)-one (5a). 2-Aminobenzoic acid and 1-benzylpiperidin-4-amine (**4a**) were used as reactants to give **5a** (0.61 g, 82%) as a white solid: mp 182.4−183.5 °C; R_f = 0.42 (10:1 CH_2Cl_2/CH_3OH); ^1H NMR (400 MHz, $CDCl_3$) δ 8.04 (d, J = 7.7 Hz, 1H), 7.63 (d, J = 7.9 Hz, 1H), 7.56 (t, J = 6.9 Hz, 1H), 7.41 (t, J = 7.1 Hz, 1H), 7.34−7.28 (m, 5H), 4.56−4.48 (m, 1H), 3.54 (s, 2H), 3.00 (d, J = 11.9 Hz, 2H), 2.20 (t, J = 11.0 Hz, 2H), 2.08−2.01 (m, 2H), 1.82−1.72 (m, 2H); ^{13}C NMR (101 MHz, $CDCl_3$) δ 166.77, 138.05, 137.94, 131.71, 129.16 (2C), 128.62, 128.28 (3C), 127.14, 126.12, 123.87, 62.94, 52.72 (2C), 52.13, 33.21 (2C); FT-IR 2922, 2803, 1591, 1446, 1340, 1251, 1019, 737, 700 cm^{-1}; HRMS (ESI) m/z [M + H]$^+$ for $C_{19}H_{20}N_2OSe$ predicted 373.0814, measured 373.0818; HPLC purity of 99.66%.

2-(1-Benzylpiperidin-4-yl)-6-fluorobenzo[d][1,2]selenazol-3(2H)-one (5b). 2-Amino-4-fluorobenzoic acid and 1-benzylpiperidin-4-amine (**4a**) were used as reactants to give **5b** (0.624 g, 80%) as a white solid: mp 199.8−201.4 °C; R_f = 0.33 (10:1 CH_2Cl_2/CH_3OH); ^1H NMR (400 MHz, $CDCl_3$) δ 8.00 (dd, J = 8.6, 5.2 Hz, 1H), 7.33−7.31 (m, 5H), 7.28 (d, J = 3.9 Hz, 1H), 7.12 (td, J = 8.6, 2.1 Hz, 1H), 4.53−4.46 (m, 1H), 3.54 (s, 2H), 2.99 (d, J = 11.9 Hz, 2H), 2.19 (t, J = 11.0 Hz, 2H), 2.04 (d, J = 9.9 Hz, 2H), 1.80−1.70 (m, 2H); ^{13}C NMR (101 MHz, $CDCl_3$) δ 165.84, 165.57 (d, J = 255.5 Hz), 139.51 (d, J = 10.1 Hz), 138.17, 130.45 (d, J = 10.1 Hz), 129.11 (2C), 128.27 (2C), 127.14, 124.66, 114.69 (d, J = 24.2 Hz), 110.81 (d, J = 26.3 Hz), 62.90, 52.67 (2C), 52.35, 33.19 (2C); FT-IR 2916, 2804, 1589, 1463, 1410, 1341, 1213, 1074, 872, 740 cm^{-1}; HRMS (ESI) m/z [M + H]$^+$ for $C_{19}H_{19}N_2OFSe$ predicted 391.0720, measured 391.0731; HPLC purity of 99.58%.

2-(1-Benzylpiperidin-4-yl)-6-chlorobenzo[d][1,2]selenazol-3(2H)-one (5c). 2-Amino-4-chlorobenzoic acid and 1-benzylpiperidin-4-amine (**4a**) were used as reactants to give **5c** (0.658 g, 81%) as a white solid: mp 217.2−219.4 °C; R_f = 0.33 (10:1 CH_2Cl_2/CH_3OH); ^1H NMR (400 MHz, $CDCl_3$) δ 7.94 (d, J = 8.4 Hz, 1H), 7.63 (s, 1H), 7.38 (d, J = 8.4 Hz, 1H), 7.34−7.28 (m, 5H), 4.55−4.45 (m, 1H), 3.54 (s, 2H), 2.99 (d, J = 12.0 Hz, 2H), 2.19 (t, J = 11.3 Hz, 2H), 2.04 (d, J = 10.2 Hz, 2H), 1.79−1.71 (m, 2H); ^{13}C NMR (101 MHz, $CDCl_3$) δ 166.87, 139.07, 138.35, 138.15, 129.53, 129.11 (2C), 128.28 (2C), 127.15, 126.99, 126.80, 123.71, 62.90, 52.65 (2C), 52.35, 33.19 (2C); FT-IR 2916, 2801, 1573, 1446, 1368, 1298, 1079, 736, 696 cm^{-1}; HRMS (ESI) m/z [M + H]$^+$ for $C_{19}H_{19}N_2OClSe$ predicted 407.0422, measured 407.0408; HPLC purity of 98.17%.

2-(1-Benzylpiperidin-4-yl)-5,6-dimethoxybenzo[d][1,2]selenazol-3(2H)-one (5d). 2-Amino-4,5-dimethoxybenzoic acid and 1-benzylpiperidin-4-amine (**4a**) were used as reactants to give **5d** (0.657 g, 76%) as a white solid: mp 177.7−180.3 °C; R_f = 0.33 (10:1 CH_2Cl_2/CH_3OH); ^1H NMR (400 MHz, $CDCl_3$) δ 7.47 (s, 1H), 7.34−7.27 (m, 5H), 7.05 (s, 1H), 4.49 (s, 1H), 3.96 (s, 6H), 3.55 (s, 2H), 3.00 (d, J =

10.0 Hz, 2H), 2.21 (t, J = 10.8 Hz, 2H), 2.03 (s, 2H), 1.76 (d, J = 12.1 Hz, 2H); ^{13}C NMR (101 MHz, $CDCl_3$) δ 166.85, 153.27, 148.92, 138.19, 130.50, 129.14 (2C), 128.25 (2C), 127.11, 120.82, 109.39, 105.23, 62.94, 56.31, 56.21, 52.73 (2C), 52.20, 33.26 (2C); FT-IR 2931, 2803, 1596, 1491, 1457, 1410, 1359, 1272, 1214, 1035, 745, 700 cm^{-1}; HRMS (ESI) m/z [M + H]$^+$ for $C_{21}H_{24}N_2O_3Se$ predicted 433.1026, measured 433.1022; HPLC purity of 98.61%.

2-[(1-Benzylpiperidin-4-yl)methyl]benzo[d][1,2]selenazol-3(2H)-one (6a). 2-Aminobenzoic acid and (1-benzylpiperidin-4-yl)methanamine (**4b**) were used as reactants to give **6a** (0.564 g, 73%) as a white solid: mp 132.7−134.8 °C; R_f = 0.31 (10:1 CH_2Cl_2/CH_3OH); ^1H NMR (400 MHz, $CDCl_3$) δ 8.04 (d, J = 7.9 Hz, 1H), 7.62−7.55 (m, 2H), 7.41 (t, J = 7.2 Hz, 1H), 7.29 (d, J = 3.1 Hz, 4H), 7.23 (d, J = 3.4 Hz, 1H), 3.74 (d, J = 5.6 Hz, 2H), 3.49 (s, 2H), 2.87 (d, J = 11.2 Hz, 2H), 1.96 (t, J = 11.5 Hz, 2H), 1.81−1.66 (m, 3H), 1.45−1.37 (m, 2H); ^{13}C NMR (101 MHz, $CDCl_3$) δ 167.37, 138.52, 137.81, 131.91 129.07, 128.97 (2C), 128.13 (2C), 127.39, 126.89, 126.17, 123.90, 63.22, 53.12 (2C), 50.37, 37.11, 29.91 (2C); FT-IR 2918, 2801, 1605, 1445, 1343, 1309, 1146, 738, 672 cm^{-1}; HRMS (ESI) m/z [M + H]$^+$ for $C_{20}H_{22}N_2OSe$ predicted 387.0971, measured 387.0970; HPLC purity of 98.90%.

2-[(1-Benzylpiperidin-4-yl)methyl]-6-fluorobenzo[d][1,2]selenazol-3(2H)-one (6b). 2-Amino-4-fluorobenzoic acid and (1-benzylpiperidin-4-yl)methanamine (**4b**) were used as reactants to give **6b** (0.606 g, 75%) as a white solid: mp 165.0−166.4 °C; R_f = 0.34 (10:1 CH_2Cl_2/CH_3OH); ^1H NMR (400 MHz, $CDCl_3$) δ 8.00 (dd, J = 8.5, 5.3 Hz, 1H), 7.34−7.28 (m, 5H), 7.25−7.20 (m, 1H), 7.13 (t, J = 8.6 Hz, 1H), 3.72 (d, J = 6.8 Hz, 2H), 3.49 (s, 2H), 2.88 (d, J = 11.2 Hz, 2H), 1.96 (t, J = 11.5 Hz, 2H), 1.71 (d, J = 11.7 Hz, 3H), 1.44−1.36 (m, 2H); ^{13}C NMR (101 MHz, $CDCl_3$) δ 166.44, 165.10 (d, J = 256.5 Hz), 139.32 (d, J = 11.1 Hz), 138.45, 130.67 (d, J = 10.1 Hz), 129.08 (2C), 128.14 (2C), 126.92, 123.71, 114.76 (d, J = 23.2 Hz), 110.85 (d, J = 26.3 Hz), 63.21, 53.09 (2C), 50.48, 37.07, 29.87 (2C); FT-IR 2921, 2803, 1602, 1463, 1417, 1340, 1245, 1174, 874, 828 cm^{-1}; HRMS (ESI) m/z [M + H]$^+$ for $C_{20}H_{21}N_2OFSe$ predicted 405.0877, measured 405.0863; HPLC purity of 99.96%.

2-[(1-Benzylpiperidin-4-yl)methyl]-6-chlorobenzo[d][1,2]selenazol-3(2H)-one (6c). 2-Amino-4-chlorobenzoic acid and (1-benzylpiperidin-4-yl)methanamine (**4b**) were used as reactants to give **6c** (0.630 g, 75%) as a white solid: mp 198.6−200.2 °C; R_f = 0.28 (10:1 CH_2Cl_2/CH_3OH); ^1H NMR (400 MHz, $CDCl_3$) δ 7.95 (d, J = 8.2 Hz, 1H), 7.62 (s, 1H), 7.43−7.36 (m, 1H), 7.34−7.23 (m, 5H), 3.73 (s, 2H), 3.49 (s, 2H), 2.88 (d, J = 9.5 Hz, 2H), 1.96 (t, J = 11.3 Hz, 2H), 1.73−1.66 (m, 3H), 1.45−1.36 (m, 2H); ^{13}C NMR (101 MHz, $CDCl_3$) δ 166.48, 138.92, 138.57, 138.44, 129.75, 129.07 (2C), 128.14 (2C), 127.05, 126.93, 125.86, 123.75, 63.21, 53.08 (2C), 50.48, 37.07, 29.87 (2C); FT-IR 2918, 2796, 1588, 1398, 1302, 1086, 753, 700 cm^{-1}; HRMS (ESI) m/z [M + H]$^+$ for $C_{20}H_{21}N_2OClSe$ predicted 421.0579, measured 421.0581; HPLC purity of 99.76%.

2-[(1-Benzylpiperidin-4-yl)methyl]-5,6-dimethoxybenzo[d][1,2]selenazol-3(2H)-one (6d). 2-Amino-4,5-dimethoxybenzoic acid and (1-benzylpiperidin-4-yl)methanamine (**4b**) were used as reactants to give **6d** (0.624 g, 70%) as a white solid: mp 165.1−166.9 °C; R_f = 0.27 (10:1 CH_2Cl_2/CH_3OH); ^1H NMR (400 MHz, $CDCl_3$) δ 7.47 (s, 1H), 7.30−7.24 (m, 5H), 7.03 (s, 1H), 3.96 (s, 3H), 3.95 (s, 3H), 3.72 (d, J = 6.5 Hz, 2H), 3.49 (s, 2H), 2.88 (d, J = 11.6 Hz, 2H), 1.97 (t, J = 11.4 Hz, 2H), 1.72 (d, J = 13.4 Hz, 3H), 1.45−1.36 (m, 2H); ^{13}C NMR (101 MHz, $CDCl_3$) δ 167.44, 153.41, 148.94, 138.45, 130.20, 129.08 (2C), 128.13 (2C), 126.90, 119.86, 109.66, 105.21, 63.22, 56.26, 56.20, 53.13 (2C), 50.42, 37.17, 29.85 (2C); FT-IR 2923, 2801, 1598, 1490, 1456, 1270, 1213, 1144, 1031, 755, 700 cm^{-1}; HRMS (ESI) m/z [M + H]$^+$ for $C_{22}H_{26}N_2O_3Se$ predicted 447.1183, measured 447.1172; HPLC purity of 98.76%.

2-[2-(1-Benzylpiperidin-4-yl)ethyl]benzo[d][1,2]selenazol-3(2H)-one (7a). 2-Aminobenzoic acid and 2-(1-benzylpiperidin-4-yl)ethanamine (**4c**) were used to give **7a** (0.536 g, 67%) as a white solid: mp 110.0−112.3 °C; R_f = 0.27 (10:1 CH_2Cl_2/CH_3OH); ^1H NMR (400 MHz, $CDCl_3$) δ 8.03 (d, J = 7.8 Hz, 1H), 7.66−7.54 (m, 2H), 7.42 (t, J = 7.4 Hz, 1H), 7.30−7.29 (m, 4H), 7.26−7.20 (m, 1H), 3.89 (t, J = 7.3 Hz, 2H), 3.48 (s, 2H), 2.87 (d, J =

11.7 Hz, 2H), 1.94 (t, J = 11.1 Hz, 2H), 1.74 (d, J = 10.3 Hz, 2H), 1.66 (dd, J = 13.8, 6.7 Hz, 2H), 1.37−1.27 (m, 3H); ^{13}C NMR (101 MHz, CDCl$_3$) δ 167.12, 138.39, 137.66, 131.86, 129.23 (2C), 128.80, 128.13 (2C), 127.62, 126.91, 126.20, 123.99, 63.42, 53.63 (2C), 42.56, 37.20, 33.14, 32.16 (2C); FT-IR 2918, 2800, 1602, 1444, 1346, 1267, 743, 702 cm^{-1}; HRMS (ESI) m/z [M + H]$^+$ for C$_{21}$H$_{24}$N$_2$OSe predicted 401.1128, measured 401.1121; HPLC purity of 98.61%.

2-[2-(1-Benzylpiperidin-4-yl)ethyl]-6-fluorobenzo[d][1,2]-selenazol-3(2H)-one (7b). 2-Amino-4-fluorobenzoic acid and 2-(1-benzylpiperidin-4-yl)ethanamine (**4c**) were used as reactants to give **7b** (0.552 g, 66%) as a white solid: mp 171.2−173.5 °C; R_f = 0.31 (10:1 CH$_2$Cl$_2$/CH$_3$OH); ^{1}H NMR (400 MHz, CDCl$_3$) δ 8.00 (dd, J = 8.5, 5.4 Hz, 1H), 7.34−7.24 (m, 5H), 7.14 (t, J = 8.7 Hz, 2H), 3.87 (t, J = 7.2 Hz, 2H), 3.48 (s, 2H), 2.87 (d, J = 10.6 Hz, 2H), 1.94 (t, J = 10.9 Hz, 2H), 1.73 (d, J = 10.4 Hz, 2H), 1.66 (s, 2H), 1.39−1.29 (m, 3H); ^{13}C NMR (101 MHz, CDCl$_3$) δ 165.16, 164.04 (d, J = 255.53 Hz), 138.06 (d, J = 10.1 Hz), 137.42, 129.59 (d, J = 9.1 Hz), 128.19 (2C), 127.10 (2C), 125.88, 122.92, 113.75 (d, J = 23.2 Hz), 109.89 (d, J = 25.3 Hz), 62.41, 52.60 (2C), 41.68, 36.14, 32.16, 31.16 (2C); FT-IR 2920, 2855, 1602, 1458, 1413, 1343, 1255, 1026, 749 cm^{-1}; HRMS (ESI) m/z [M + H]$^+$ for C$_{21}$H$_{23}$N$_2$OFSe predicted 419.1033, measured 419.1023; HPLC purity of 96.14%.

2-[2-(1-Benzylpiperidin-4-yl)ethyl]-6-chlorobenzo[d][1,2]-selenazol-3(2H)-one (7c). 2-Amino-4-chlorobenzoic acid and 2-(1-benzylpiperidin-4-yl)ethanamine (**4c**) were used as reactants to give **7c** (0.547 g, 63%) as a white solid: mp 194.2−196.8 °C; R_f = 0.31 (10:1 CH$_2$Cl$_2$/CH$_3$OH); ^{1}H NMR (400 MHz, CDCl$_3$) δ 7.94 (d, J = 8.1 Hz, 1H), 7.68 (s, 1H), 7.39 (s, 1H), 7.29 (s, 4H), 7.25 (s, 1H), 3.87 (d, J = 13.0 Hz, 2H), 3.47 (s, 2H), 2.86 (s, 2H), 1.93 (s, 2H), 1.71−1.62 (m, 4H), 1.33 (s, 3H); ^{13}C NMR (101 MHz, CDCl$_3$) δ 166.21, 138.77, 138.49, 138.43, 129.66, 129.21 (2C), 128.13 (2C), 127.06, 126.91, 126.11, 123.83, 63.42, 53.61 (2C), 42.69, 37.16, 33.18, 32.17 (2C); FT-IR 2913, 2846, 1584, 1448, 1398, 1300, 1085, 736, 697 cm^{-1}; HRMS (ESI) m/z [M + H]$^+$ for C$_{21}$H$_{23}$N$_2$OClSe predicted 435.0735, measured 435.0731; HPLC purity of 97.2%.

2-[2-(1-Benzylpiperidin-4-yl)ethyl]-5,6-dimethoxybenzo[d][1,2]-selenazol-3(2H)-one (7d). 2-Amino-4,5-dimethoxybenzoic acid and 2-(1-benzylpiperidin-4-yl)ethanamine (**4c**) were used as reactants to give **7d** (0.561 g, 61%) as a white solid: mp 175.1−177.2 °C; R_f = 0.31 (10:1 CH$_2$Cl$_2$/CH$_3$OH); ^{1}H NMR (400 MHz, CDCl$_3$) δ 7.46 (s, 1H), 7.30 (s, 2H), 7.29 (s, 2H), 7.25−7.22 (m, 1H), 7.04 (s, 1H), 3.96 (s, 3H), 3.95 (s, 3H), 3.87 (t, J = 7.2 Hz, 2H), 3.48 (s, 2H), 2.87 (d, J = 11.7 Hz, 2H), 1.94 (t, J = 11.2 Hz, 2H), 1.74 (d, J = 10.4 Hz, 2H), 1.68−1.65 (m, 2H), 1.37−1.29 (m, 3H); ^{13}C NMR (101 MHz, CDCl$_3$) δ 167.19, 153.35, 148.95, 138.44, 130.10, 129.21 (2C), 128.10 (2C), 126.88, 120.14, 109.60, 105.35, 63.43, 56.32, 56.20, 53.64 (2C), 42.65, 37.28, 33.14, 32.19 (2C); FT-IR 2920, 2801, 1597, 1490, 1456, 1413, 1352, 1270, 1214, 1146, 1031, 866, 738, 699 cm^{-1}; HRMS (ESI) m/z [M + H]$^+$ for C$_{23}$H$_{28}$N$_2$O$_3$Se predicted 461.1339, measured 461.1340; HPLC purity of 97.07%.

2-[3-(1-Benzylpiperidin-4-yl)propyl]-5,6-dimethoxybenzo[d][1,2]-selenazol-3(2H)-one (8). 2-Amino-4,5-dimethoxybenzoic acid and 3-(1-benzylpiperidin-4-yl)propan-1-amine (**4d**) were used as reactants to give **8** (0.521 g, 55%) as a white solid: mp 151.1−152.4 °C; R_f = 0.33 (10:1 CH$_2$Cl$_2$/CH$_3$OH); ^{1}H NMR (400 MHz, CDCl$_3$) δ 7.47 (d, J = 3.1 Hz, 1H), 7.30−7.27 (m, 5H), 7.04 (d, J = 3.1 Hz, 1H), 3.96 (s, 6H), 3.81 (s, 2H), 3.48 (d, J = 2.9 Hz, 2H), 2.86 (d, J = 10.3 Hz, 2H), 1.93 (t, J = 9.9 Hz, 2H), 1.72 (s, 2H), 1.65 (s, 4H), 1.32−1.29 (m, 3H); ^{13}C NMR (101 MHz, CDCl$_3$) δ 167.24, 153.32, 148.91, 138.55, 130.14, 129.20 (2C), 128.09 (2C), 126.85, 120.11, 109.56, 105.34, 63.49, 56.31, 56.19, 53.84 (2C), 45.06, 35.46, 33.30, 32.26 (2C), 27.94; FT-IR 2923, 2850, 1598, 1490, 1456, 1419, 1270, 1144, 1030, 867, 740 cm^{-1}; HRMS (ESI) m/z [M + H]$^+$ for C$_{24}$H$_{30}$N$_2$O$_3$Se predicted 475.1496, measured 475.1468; HPLC purity of 98.86%.

2-[4-(1-Benzylpiperidin-4-yl)butyl]-5,6-dimethoxybenzo[d][1,2]-selenazol-3(2H)-one (9). 2-Amino-4,5-dimethoxybenzoic acid and 4-(1-benzylpiperidin-4-yl)butan-1-amine (**4e**) were used as reactants to give **9** (0.566 g, 58%) as a white solid: mp 141.4−144.2 °C; R_f = 0.31 (10:1 CH$_2$Cl$_2$/CH$_3$OH); ^{1}H NMR (400 MHz, CDCl$_3$) δ 7.46 (s, 1H), 7.30 (d, J = 3.8 Hz, 4H), 7.25−7.20 (m, 1H), 7.04 (s, 1H), 3.95 (s, 6H), 3.82 (t, J = 7.0 Hz, 2H), 3.47 (s, 2H), 2.85 (d, J = 10.3 Hz, 2H), 1.93−1.88 (m, 3H), 1.70−1.61 (m, 4H), 1.39 (s, 2H), 1.22−1.26 (m, 4H); ^{13}C NMR (101 MHz, CDCl$_3$) δ 167.22, 153.33, 148.93, 138.53, 130.10, 129.23 (2C), 128.09 (2C), 126.85, 120.13, 109.60, 105.31, 63.51, 56.31, 56.20, 53.90 (2C), 44.90, 36.20, 35.59, 32.32 (2C), 30.86, 23.82; FT-IR 2923, 2851, 1598, 1490, 1450, 1270, 1214, 1145, 1030, 754 cm^{-1}; HRMS (ESI) m/z [M + H]$^+$ for C$_{25}$H$_{32}$N$_2$O$_3$Se predicted 489.1652, measured 489.1623; HPLC purity of 98.50%.

2-[2-(1-Benzylpiperidin-4-yl)ethyl]-5,6-dimethoxybenzo[d][1,2]-selenazol-3(2H)-one 1-Oxide (10). A solution of 30% H$_2$O$_2$ (65 μL, 0.65 mmol) was added to a solution of **7d** (0.2 g, 0.43 mmol) in 10 mL of CH$_2$Cl$_2$, which was stirred for 30 min at room temperature. After the reaction was complete, the solvents were evaporated under vacuum, and the crude product was purified by column chromatography to provide a colorless oil (0.133 g, 65%): R_f = 0.21 (10:1 CH$_2$Cl$_2$/CH$_3$OH); ^{1}H NMR (400 MHz, DMSO) δ 7.78 (d, J = 5.2 Hz, 1H), 7.32 (s, 6H), 3.90 (t, J = 5.5 Hz, 6H), 3.80−3.71 (m, 1H), 3.68−3.52 (m, 3H), 2.83 (s, 2H), 1.99 (s, 2H), 1.71 (s, 2H), 1.59 (s, 2H), 1.24 (s, 3H); ^{13}C NMR (101 MHz, DMSO) δ 168.06, 152.87, 151.87, 139.27, 130.03, 129.07 (2C), 128.14 (2C), 127.13, 123.58, 109.57, 108.37, 62.04, 56.16, 56.01 (2C), 52.81, 48.09, 36.08, 32.39, 31.21 (2C); FT-IR 2923, 2809, 1589, 1490, 1448, 1422, 1271, 1214, 1045, 843 cm^{-1}; HRMS (ESI) m/z [M + H]$^+$ for C$_{23}$H$_{28}$N$_2$O$_4$Se predicted 477.1288, measured 477.1276; HPLC purity of 96.0%.

Biological Assays. *Determination of the Inhibitory Effects on eeAChE, BuChE, and hAChE Activities.* We followed the method of Ellman et al. Acetylcholinesterase (from electric eel or human erythrocytes), butyrylcholinesterase (from equine serum), 5,5′-dithiobis(2-nitrobenzoic acid) (DTNB), acetylthiocholine chloride (ATC), and butyrylthiocholine chloride (BTC) were purchased from Sigma-Aldrich. The prototypes tacrine and donepezil were used as reference compounds. Five different concentrations of each compound were used to obtain between 20 and 80% inhibition of cholinesterase activity.

All assays were conducted in 0.1 M KH$_2$PO$_4$/K$_2$HPO$_4$ buffer at pH 8.0 using a Shimadzu UV-2450 spectrophotometer. AChE solutions were prepared to produce concentrations of 2.0 units/mL in 2 mL aliquots. The assay medium (1 mL) consisted of phosphate buffer (pH 8.0), 50 μL of 0.01 M DTNB, and 20 μL of AChE (from electric eel or human serum). The test compounds were added to the assay solution and preincubated at 37 °C for 15 min, and 50 μL of 0.01 M ATC was added immediately. The activity was determined by measuring the increase in absorbance at 412 nm at 1 min intervals at 37 °C. Data from concentration−inhibition experiments with the inhibitors were subjected to nonlinear regression analysis using GraphPad Prism version 5.0 (GraphPad Software Inc.), which gave estimates of the IC$_{50}$ (concentration of the drug resulting in 50% inhibition of enzyme activity).

Inhibition of BuChE was measured as described above, substituting 0.02 M BTC for the substrate.

Kinetic Characterization of AChE Inhibition. Kinetic characterization of AChE was performed using the reported method. The test compound was added to the assay solution and preincubated with the enzyme at 37 °C for 15 min, followed by the addition of substrate (0.1−1.0 mM). Kinetic characterization of the hydrolysis of ATC catalyzed by AChE was performed spectrometrically at 412 nm. A parallel control with no inhibitor in the mixture allowed the activities measured at various times to be adjusted. The plots were assessed by a weighted least-squares analysis that assumed the variance of V to be a constant percentage of V for the entire data set. The slopes of these reciprocal plots were then plotted against the concentrations of the inhibitors in a weighted analysis, and K_i was determined as the ratio of the replot intercept to the replot slope.

Inhibition of Human Recombinant AChE-Induced A$\beta_{1−40}$ Peptide Aggregation Assay. The thioflavin T (ThT) fluorescence method was used as previously described.[42] A$\beta_{1−40}$ (Sigma-Aldrich), lyophilized from a 2 mg/mL 1,1,1,3,3,3-hexafluoro-2-propanol (HFIP) solution, and a test compound were dissolved in DMSO to produce 2.3 mM and 1 mM solutions. Two microliters of A$\beta_{1−40}$ was incubated with 16 μL of human recombinant AChE (Sigma-Aldrich) in the presence of 2

μL of a test compound to give final concentrations of 230 μM Aβ$_{1-40}$, 2.3 μM hAChE, and 100 μM test compound. Following co-incubation at room temperature for 48 h, 180 μL of 1.5 μM ThT in 50 mM glycine-NaOH buffer (pH 8.5) was added. The fluorescence was monitored at 446 nm, and the emission was monitored at 490 nm using a Molecular Devices SpectraMax spectrofluorometer. The percent inhibition of the AChE-induced aggregation was calculated by the following expression: $100 - (IF_i/IF_0 \times 100)$, where IF_i and IF_0 are the fluorescence intensities in the presence and absence of the test compound, respectively, minus the fluorescence intensities due to the respective blanks. Each assay was conducted in triplicate, and each experiment was repeated at least three independent times.

Coupled Reductase Assay. The GPx-like activity of the organo-selenium compounds was determined using a spectrophotometric method at 340 nm as described by Wilson et al.[27] The test mixture contained GSH (2 mM), EDTA (1 mM), glutathione reductase (1.3 units/mL), and NADPH (0.4 mM) in 100 mM potassium phosphate buffer (pH 7.5). GPx samples (80 μM) were added to the test mixture at 25 °C, and the reaction was initiated by the addition of H$_2$O$_2$ (1.6 mM). The initial reduction rates were calculated from the oxidation rate of NADPH at 340 nm. The initial reduction rate was determined at least three times and calculated from the first 5−10% of the reaction using a value of 6.22 mM^{-1} cm^{-1} as the extinction coefficient for NADPH.

FOX Assay. The hydrogen peroxide scavenging activity was determined by the ferrous ion oxidation−xylenol orange (FOX) assay with minor changes. FOX reagent was prepared by adding 9 volumes of reagent **1** to 1 volume of reagent **2**, where reagent **1** was 4.4 mM butylated hydroxytoluene (BHT) in methanol and reagent **2** was 1 mM xylenol orange and 2.56 mM ammonium ferrous sulfate in 250 μM H$_2$SO$_4$. Test compounds (400 μL) at different concentrations were incubated with 1 mM H$_2$O$_2$ (100 μL) for 10 h at 37 °C in the dark, and the FOX agent (500 μL) was added. The reaction mixture was then vortexed and incubated at room temperature for 30 min. The development of violet color indicated a positive control reaction, and discoloration was considered scavenging activity after addition of the test compound. The FOX reagent without compound or H$_2$O$_2$ served as a blank or control. The absorbance of the ferric−xylenol orange complex was measured at 560 nm.

Peroxynitrite Scavenging Activity. Peroxynitrite, whose formation results in the bleaching of Evans blue (EB) dye, was measured at 608 nm (ε = 70000 M^{-1} cm^{-1}). Consumption of Evans blue dye, without or with different concentrations of test compound, was the basis for the calculated amount of peroxynitrite. D_0 and D_{TC} are the stoichiometries for the reaction of peroxynitrite with Evans blue dye without and with the test compound, respectively. The k_{TC}/k_{EB} ratio could be calculated from the slope of the straight line plotting $\Delta[TC]_0/\Delta[EB]$ versus $[TC]/[EB]$. For the sake of simplicity, initial concentrations $[TC]_0$ and $[EB]_0$ were used in the calculations. In this work, instead of $\Delta[EB]$, we measured the stoichiometry $D = \Delta[EB]/\Delta[NaOONO^{3-}]$ to avoid the effect of slight deviations in peroxynitrite concentration. The ratio D_0/D_{TC} is equivalent to $\Delta[TC]_0/\Delta[EB]_a$, where D_0 and D_{TC} are the reaction stoichiometries in the absence and presence of the test compound, respectively. The antioxidant activity was measured as the slope of the straight line (k_{TC}/k_{EB}).

Peroxynitrite synthesis was conducted by modifying the method described by Beckman et al.[44] Acidified H$_2$O$_2$ (8.2 M in 1.85 M HNO$_3$, 6.6 mL) and sodium nitrite (2 M, 6 mL) solutions were drawn into two separate syringes. The contents of both syringes were simultaneously injected into an ice-cooled beaker containing 4.2 M sodium hydroxide (6 mL) through a Y-shaped junction. Excess hydrogen peroxide was removed by MnO$_2$ treatment. The concentration of the resultant stock solution was measured spectrophotometrically at 302 nm (ε = 1670 M^{-1} cm^{-1}). The typical yield ranged from 70 to 80 mM. Peroxynitrite was used to induce the bleaching of Evans blue dye, which was measured at 608 nm (ε = 70000 M^{-1} cm^{-1}). Consumption of Evans blue (20 μM) in the absence and presence of the different concentrations of the test compound was measured over the peroxynitrite (20 μM). Antioxidant activities were determined against the control.

Substrates for Hepatic Mammalian Thioredoxin Reductase (TrxR). TrxR activity was determined according to the method of Zhao and Holmgren.[21] Measurements of TrxR activity were performed in a buffer containing 140 μL of 50 mM Tris-HCl, 1 mM EDTA (pH 7.5), 20 μL of NADPH (1 mM), and 20 μL of the test compound (150 μM). Reactions were initiated by the addition of 20 μL of TrxR (3.5 units/mL), and the absorbance at 340 nm was monitored for 10 min.

In Vitro Blood−Brain Barrier Permeation Assay. Brain penetration of compounds was evaluated using a parallel artificial membrane permeation assay (PAMPA), in a manner similar to that described by Di et al.[44] as the basis for the calculated amount of peroxynitrite. Commercial drugs were purchased from Sigma and Alfa Aesar. Porcine brain lipid (PBL) was obtained from Avanti Polar Lipids. The donor microplate (PVDF membrane, pore size of 0.45 mm) and the acceptor microplate were both from Millipore. The 96-well UV plate (COSTAR) was obtained from Corning Inc. The acceptor 96-well microplate was filled with 300 μL of a PBS/EtOH mixture (7:3), and the filter membrane was impregnated with 4 μL of PBL in dodecane (20 mg/mL). The compound was dissolved in DMSO at a concentration of 5 mg/mL and diluted 50-fold in a PBS/EtOH mixture (7:3) to yield a concentration of 100 mg/mL, and 200 μL was added to the donor wells. The acceptor filter plate was carefully placed on the donor plate to form a sandwich, which was left undisturbed for 10 h at 25 °C. After incubation, the donor plate was carefully removed, and the concentrations of the compound in the acceptor wells were determined using a UV plate reader (Flexstation 3). Every sample was analyzed at five wavelengths in four wells and in at least three independent runs, and the results are given as the means ± standard deviation (Table S8 of the Supporting Information). In each experiment, 13 quality control standards of known BBB permeability were included to validate the analysis set. A plot of the experimental data versus literature values gave a good linear correlation, P_e(exp) = $1.4574P_e$(bibl) $- 1.0773$ (R^2 = 0.9427) (Figure S1 of the Supporting Information). From this equation and considering the limit established by Di et al. for blood−brain barrier permeation, we found that compounds with permeabilities above 4.7×10^{-6} cm s^{-1} are able to cross the blood−brain barrier (Table S9 of the Supporting Information).

Acute Toxicity of Compound 7d. Twenty KM mice (22 days, 18−20 g), purchased from the laboratory animal center of Sun Yat-sen University (Guangzhou, China), were used to evaluate the acute toxicity of compound **7d**. Mice were maintained on a 12 h light/dark cycle (light from 7:00 a.m. to 7:00 p.m.) at 20−22 °C and 60−70% relative humidity. Sterile food and water were provided according to institutional guidelines. Prior to each experiment, mice were fasted overnight and allowed free access to water. Compound **7d** was dissolved in a 0.5% carboxymethyl cellulose sodium (CMC-Na) salt solution and given via oral administration to different experimental groups. After administration of the compound, mice were observed continuously for the first 4 h for any abnormal behavior and mortality changes, intermittently for the next 24 h, and occasionally thereafter for 14 days for the onset of any delayed effects. All animals were sacrificed on the 14th day after drug administration and macroscopically evaluated for possible damage to the heart, liver, and kidneys.

■ ASSOCIATED CONTENT

⑤ Supporting Information

Experimental procedures for the synthesis of the amine intermediates (**4a−e**), the HPLC data and FT-IR spectra of the target compounds, the full data regarding the GPx-like activity of the test compounds, and the method for PAMPA. This material is available free of charge via the Internet at http://pubs.acs.org.

■ AUTHOR INFORMATION

Corresponding Authors
*Phone: +086-20-3994-3051. Fax: +086-20-3994-3051. E-mail: Huangl72@mail.sysu.edu.cn.
*Phone: +086-20-3994-3050. Fax: +086-20-3994-3050. E-mail: lixsh@mail.sysu.edu.cn.

Notes
The authors declare no competing financial interest.

■ ABBREVIATIONS USED

AD, Alzheimer's disease; AChE, acetylcholinesterase; hAChE, human acetylcholinesterase; BuChE, butyrylcholinesterase; GPx, glutathione peroxidase; CNS, central nervous system; Aβ, β-amyloid; AChEIs, acetyl cholinesterase inhibitors; MTDLs, multi-target-directed ligands; PAS, peripheral anionic site; CAS, catalytic binding site; GSH, glutathione; EDTA, ethylenediaminetetraacetate; GR, glutathione reductase; ROS, reactive oxygen species; FOX, ferrous ion oxidation–xylenol orange; EB, Evans blue; PAMPA-BBB, parallel artificial membrane permeation assay for the blood–brain barrier; DTNB, 5,5′-dithiobis(2-nitrobenzoic acid); ATC, acetylthiocholine chloride; BTC, butyrylthiocholine chloride; ThT, thioflavin T; TLC, thin-layer chromatography; PBL, porcine brain lipid; SD, standard deviation

■ REFERENCES

(1) Martin, P.; Jim, J. *World Alzheimer Report 2012*; Alzheimer's Disease International: London, 2012; pp 1−75.

(2) Scarpini, E.; Schelterns, P.; Feldman, H. Treatment of Alzheimer's disease; current status and new perspectives. *Lancet Neurol.* **2003**, 2, 539−547.

(3) Van der Zee, E. A.; Platt, B.; Riedel, G. Acetylcholine: Future research and perspectives. *Behav. Brain Res.* **2011**, 221, 583−586.

(4) Sugimoto, H.; Yamanish, Y.; Iimura, Y.; Kawakami, Y. Donepezil Hydrochloride (E2020) and Other Acetylcholinesterase Inhibitors. *Curr. Med. Chem.* **2000**, 7, 303−339.

(5) Cavalli, A.; Bolognesi, M. L.; Minarini, A.; Rosini, M.; Tumiatti, V.; Recanatini, M.; Melchiorre, C. Multi-target-Directed Ligands To Combat Neurodegenerative Diseases. *J. Med. Chem.* **2008**, 51, 347−372.

(6) Youdim, M. B.; Buccafusco, J. J. Multi-functional drugs for various CNS targets in the treatment of neurodegenerative disorders. *Trends Pharmacol. Sci.* **2005**, 26, 27−35.

(7) Sterling, J.; Herzig, Y.; Goren, T.; Finkelstein, N.; Lerner, D.; Goldenberg, W.; Miskolczi, I.; Molnar, S.; Rantal, F.; Tamas, T.; Toth, G.; Zagyva, A.; Zekany, A.; Finberg, J.; Lavian, G.; Gross, A.; Friedman, R.; Razin, M.; Huang, W.; Krais, B.; Chorev, M.; Youdim, M. B.; Weinstock, M. Novel dual inhibitors of AChE and MAO derived from hydroxy aminoindan and phenethylamine as potential treatment for Alzheimer's disease. *J. Med. Chem.* **2002**, 45, 5260−5279.

(8) León, R.; Garcia, A. G.; Marco-Contelles, J. Recent advances in the multitarget-directed ligands approach for the treatment of Alzheimer's disease. *Med. Res. Rev.* **2013**, 33, 139−189.

(9) Bartolini, M.; Pistolozzi, M.; Andrisano, V.; Egea, J.; López, M. G.; Iriepa, I.; Moraleda, I.; Gálvez, E.; Marco-Contelles, J.; Samadi, A. Chemical and Pharmacological Studies on Enantiomerically Pure p-Methoxytacripyrines, Promising Multi-Target-Directed Ligands for the Treatment of Alzheimer's Disease. *ChemMedChem* **2011**, 6, 1990−1997.

(10) Samadi, A.; Estrada, M.; Pérez, C.; Rodríguez-Franco, M. I.; Iriepa, I.; Moraleda, I.; Chioua, M.; Marco-Contelles, J. Pyridonepezils, new dual AChE inhibitors as potential drugs for the treatment of Alzheimer's disease: Synthesis, biological assessment, and molecular modeling. *Eur. J. Med. Chem.* **2012**, 57, 296−301.

(11) Buccafusco, J. J.; Terry, A. V. Multiple Central Nervous System Targets for Eliciting Beneficial Effects on Memory and Cognition. *J. Pharmacol. Exp. Ther.* **2000**, 295, 438−446.

(12) Samadi, A.; Marco-Contelles, J.; Soriano, E.; Alvarez-Perez, M.; Chioua, M.; Romero, A.; Gonzalez-Lafuente, L.; Gandia, L.; Roda, J. M.; Lopez, M. G.; Villarroya, M.; Garcia, A. G.; Rios Cde, L. Multipotent drugs with cholinergic and neuroprotective properties for the treatment of Alzheimer and neuronal vascular diseases. I. Synthesis, biological assessment, and molecular modeling of simple and readily available 2-aminopyridine-, and 2-chloropyridine-3,5-dicarbonitriles. *Bioorg. Med. Chem.* **2010**, 18, 5861−5872.

(13) Rosini, M.; Andrisano, V.; Bartolini, M.; Bolognesi, M. L.; Hrelia, P.; Minarini, A.; Tarozzi, A.; Melchiorre, C. Rational Approach To Discover Multipotent Anti-Alzheimer Drugs. *J. Med. Chem.* **2005**, 48, 360−363.

(14) Bolognesi, M. L.; Bartolini, M.; Tarozzi, A.; Morroni, F.; Lizzi, F.; Milelli, A.; Minarini, A.; Rosini, M.; Hrelia, P.; Andrisano, V.; Melchiorre, C. Multitargeted drugs discovery: Balancing anti-amyloid and anticholinesterase capacity in a single chemical entity. *Bioorg. Med. Chem. Lett.* **2011**, 21, 2655−26558.

(15) Fernández-Bachiller, M. a. I.; Pérez, C. n.; González-Muñoz, G. C.; Conde, S.; López, M. G.; Villarroya, M.; García, A. G.; Rodríguez-Franco, M. a. I. Novel Tacrine-8-Hydroxyquinoline Hybrids as Multifunctional Agents for the Treatment of Alzheimer's Disease, with Neuroprotective, Cholinergic, Antioxidant, and Copper-Complexing Properties. *J. Med. Chem.* **2010**, 53, 4927−4937.

(16) Kryukov, G. V.; Castellano, S.; Novoselov, S. V.; Lobanov, A. V.; Zehtab, O.; Guigó, R.; Gladyshev, V. N. Characterization of Mammalian Selenoproteomes. *Science* **2003**, 300, 1439−1443.

(17) Allmang, C.; Wurth, L.; Krol, A. The selenium to selenoprotein pathway in eukaryotes: More molecular partners than anticipated. *Biochim. Biophys. Acta* **2009**, 1790, 1415−14123.

(18) Berr, C.; Nicole, A.; Godin, J.; Ceballos-Picot, I.; Thevenin, M.; Dartigues, J. F.; Alperovitch, A. Selenium and oxygen-metabolizing enzymes in elderly community residents: A pilot epidemiological study. *J. Am. Geriatr. Soc.* **1993**, 41, 143−148.

(19) Savarino, L.; Granchi, D.; Ciapetti, G.; Cenni, E.; Ravaglia, G.; Forti, P.; Maioli, F.; Mattioli, R. Serum concentrations of zinc and selenium in elderly people: Results in healthy nonagenarians/centenarians. *Exp. Gerontol.* **2001**, 36, 327−339.

(20) Rayman, M. P. The importance of selenium to human health. *Lancet* **2000**, 356, 233−241.

(21) Papp, L. V.; Lu, J.; Holmgren, A.; Khanna, K. K. From selenium to selenoproteins: Synthesis, identity, and their role in human health. *Antioxid. Redox Signaling* **2007**, 9, 775−806.

(22) Zhang, S.; Rocourt, C.; Cheng, W. H. Selenoproteins and the aging brain. *Mech. Ageing Dev.* **2010**, 131, 253−260.

(23) Berr, C.; Akbaraly, T.; Arnaud, J.; Hininger, I.; Roussel, A. M.; Barberger Gateau, P. Increased selenium intake in elderly high fish consumers may account for health benefits previously ascribed to omega-3 fatty acids. *J. Nutr., Health Aging* **2009**, 13, 14−18.

(24) Mahan, D. C. Effect of organic and inorganic selenium sources and levels on sow colostrum and milk selenium content. *J. Anim. Sci.* **2000**, 78, 100−105.

(25) Pinton, S.; Bruning, C. A.; Sartori Oliveira, C. E.; Prigol, M.; Nogueira, C. W. Therapeutic effect of organoselenium dietary supplementation in a sporadic dementia of Alzheimer's type model in rats. *J. Nutr. Biochem.* **2013**, 24, 311−317.

(26) Stangherlin, E. C.; Luchese, C.; Pinton, S.; Rocha, J. B.; Nogueira, C. W. Sub-chronical exposure to diphenyl diselenide enhances acquisition and retention of spatial memory in rats. *Brain Res.* **2008**, 1201, 106−113.

(27) Wilson, S. R.; Zucker, P. A.; Huang, R. R. C.; Spector, A. Development of synthetic compounds with glutathione peroxidase activity. *J. Am. Chem. Soc.* **1989**, *111*, 5936−5939.

(28) Zhao, R.; Holmgren, A. A novel antioxidant mechanism of ebselen involving ebselen diselenide, a substrate of mammalian thioredoxin and thioredoxin reductase. *J. Biol. Chem.* **2002**, *277*, 39456−39462.

(29) Zhao, R.; Masayasu, H.; Holmgren, A. Ebselen: A substrate for human thioredoxin reductase strongly stimulating its hydroperoxide reductase activity and a superfast thioredoxin oxidant. *Proc. Natl. Acad. Sci. U.S.A.* **2002**, *99*, 8579−8584.

(30) De Freitas, A. S.; Rocha, J. B. Diphenyl diselenide and analogs are substrates of cerebral rat thioredoxin reductase: A pathway for their neuroprotective effects. *Neurosci. Lett.* **2011**, *503*, 1−5.

(31) Xie, L.; Zheng, W.; Xin, N.; Xie, J.-W.; Wang, T.; Wang, Z.-Y. Ebselen inhibits iron-induced tau phosphorylation by attenuating DMT1 up-regulation and cellular iron uptake. *Neurochem. Int.* **2012**, *61*, 334−340.

(32) Bolea, I.; Juárez-Jiménez, J.; de los Ríos, C.; Chioua, M.; Pouplana, R.; Luque, F. J.; Unzeta, M.; Marco-Contelles, J.; Samadi, A. Synthesis, Biological Evaluation, and Molecular Modeling of Donepezil and N-[(5-(Benzyloxy)-1-methyl-1H-indol-2-yl)methyl]-N-methyl-prop-2-yn-1-amine Hybrids as New Multipotent Cholinesterase/ Monoamine Oxidase Inhibitors for the Treatment of Alzheimer's Disease. *J. Med. Chem.* **2011**, *54*, 8251−8270.

(33) Ellman, G. L.; Courtney, K. D.; Andres, V., Jr.; Featherstone, R. M. A new and rapid colorimetric determination of acetylcholinesterase activity. *Biochem. Pharmacol.* **1961**, *7*, 88−95.

(34) Darvesh, S.; Hopkins, D. A.; Geula, C. Neurobiology of butyrylcholinesterase. *Nat. Rev. Neurosci.* **2003**, *4*, 131−138.

(35) Eskander, M. F.; Nagykery, N. G.; Leung, E. Y.; Khelghati, B.; Geula, C. Rivastigmine is a potent inhibitor of acetyl- and butyrylcholinesterase in Alzheimer's plaques and tangles. *Brain Res.* **2005**, *1060*, 144−152.

(36) Decker, M.; Krauth, F.; Lehmann, J. Novel tricyclic quinazolinimines and related tetracyclic nitrogen bridgehead compounds as cholinesterase inhibitors with selectivity towards butyrylcholinesterase. *Bioorg. Med. Chem.* **2006**, *14*, 1966−1977.

(37) Decker, M. Homobivalent Quinazolinimines as Novel Nanomolar Inhibitors of Cholinesterases with Dirigible Selectivity toward Butyrylcholinesterase. *J. Med. Chem.* **2006**, *49*, 5411−5413.

(38) Kryger, G.; Silman, I.; Sussman, J. L. Structure of Acetylcholinesterase Complexed with E2020 (Aricept): Implications for the Design of New Anti-Alzheimer Drugs. *Structure* **1999**, *7*, 297−307.

(39) Alvarez, A.; Bronfman, F.; Pérez, C. A.; Vicente, M.; Garrido, J.; Inestrosa, N. C. Acetylcholinesterase, a senile plaque component, affects the fibrillogenesis of amyloid-β-peptides. *Neurosci. Lett.* **1995**, *201*, 49−52.

(40) Alvarez, A.; Opazo, C.; Alarcón, R.; Garrido, J.; Inestrosa, N. C. Acetylcholinesterase promotes the aggregation of amyloid-β-peptide fragments by forming a complex with the growing fibrils. *J. Mol. Biol.* **1997**, *272*, 348−361.

(41) Inestrosa, N. C.; Alvarez, A.; Pérez, C. A.; Moreno, R. D.; Vicente, M.; Linker, C.; Casanueva, O. I.; Soto, C.; Garrido, J. Acetylcholinesterase accelerates assembly of amyloid-β-peptides into Alzheimer's fibrils: Possible role of the peripheral site of the enzyme. *Neuron* **1996**, *16*, 881−891.

(42) Bartolini, M.; Bertucci, C.; Cavrini, V.; Andrisano, V. β-Amyloid aggregation induced by human acetylcholinesterase: Inhibition studies. *Biochem. Pharmacol.* **2003**, *65*, 407−416.

(43) Gul, M. Z.; Bhakshu, L. M.; Ahmad, F.; Kondapi, A. K.; Qureshi, I. A.; Ghazi, I. A. Evaluation of *Abelmoschus moschatus* extracts for antioxidant, free radical scavenging, antimicrobial and antiproliferative activities using in vitro assays. *BMC Complementary Altern. Med.* **2011**, *11*, 64.

(44) Ischiropoulos, H.; Zhu, L.; Beckman, J. S. Peroxynitrite formation from macrophage-derived nitric oxide. *Arch. Biochem. Biophys.* **1992**, *298*, 446−451.

(45) Kooy, N. W.; Royall, J. A. Agonist-Induced Peroxynitrite Production from Endothelial Cells. *Arch. Biochem. Biophys.* **1994**, *310*, 352−359.

(46) Salgo, M. G.; Bermudez, E.; Squadrito, G. L.; Pryor, W. A. DNA Damage and Oxidation of Thiols Peroxynitrite Causes in Rat Thymocytes. *Arch. Biochem. Biophys.* **1995**, *322*, 500−505.

(47) Douki, T.; Cadet, J.; Ames, B. N. An Adduct between Peroxynitrite and 2′-Deoxyguanosine: 4,5-Dihydro-5-hydroxy-4-(nitrosooxy)-2′-deoxyguanosine. *Chem. Res. Toxicol.* **1996**, *9*, 3−7.

(48) Celia, Q.; Beatriz, A.; Reynaldo, M. G.; Ohara, A.; Rafael, R. Pathways of peroxynitrite oxidation of thiol groups. *Biochem. J.* **1997**, *322*, 167−173.

(49) Radi, R.; Beckman, J. S.; Bush, K. M.; Freeman, B. A. Peroxynitrite-induced membrane lipid peroxidation: The cytotoxic potential of superoxide and nitric oxide. *Arch. Biochem. Biophys.* **1991**, *288*, 481−487.

(50) Ramezanian, M. S.; Padmaja, S.; Koppenol, W. H. Nitration and Hydroxylation of Phenolic Compounds by Peroxynitrite. *Chem. Res. Toxicol.* **1996**, *9*, 232−240.

(51) Balavoine, G. G. A.; Geletii, Y. V. Peroxynitrite Scavenging by Different Antioxidants. Part I: Convenient Assay. *Nitric Oxide* **1999**, *3*, 40−54.

(52) Steinbrenner, H.; Sies, H. Protection against reactive oxygen species by selenoproteins. *Biochim. Biophys. Acta* **2009**, *1790*, 1478−1485.

(53) Sausen de Freitas, A.; de Souza Prestes, A.; Wagner, C.; Haigert Sudati, J.; Alves, D.; Oliveira Porciúncula, L.; Kade, I. J.; Teixeira Rocha, J. B. Reduction of Diphenyl Diselenide and Analogs by Mammalian Thioredoxin Reductase Is Independent of Their Gluthathione Peroxidase-Like Activity: A Possible Novel Pathway for Their Antioxidant Activity. *Molecules* **2010**, *15*, 7699−7714.

(54) Mugesh, G.; du Mont, W.-W.; Sies, H. Chemistry of Biologically Important Synthetic Organoselenium Compounds. *Chem. Rev.* **2001**, *101*, 2125−2180.

(55) Luchese, C.; Nogueira, C. W. Diphenyl diselenide in its selenol form has dehydroascorbate reductase and glutathione S-transferase-like activity dependent on the glutathione content. *J. Pharm. Pharmacol.* **2010**, *62*, 1146−1151.

(56) Nogueira, C. W.; Rocha, J. B. Toxicology and pharmacology of selenium: Emphasis on synthetic organoselenium compounds. *Arch. Toxicol.* **2011**, *85*, 1313−1359.

(57) Di, L.; Kerns, E. H.; Fan, K.; McConnell, O. J.; Carter, G. T. High throughput artificial membrane permeability assay for blood−brain barrier. *Eur. J. Med. Chem.* **2003**, *38*, 223−232.